InSb(100) reconstructions probed with core-level photoemission

P. John, T. Miller, and T.-C. Chiang
Department of Physics and Materials Research Laboratory, University of Illinois at Urbana-Champaign, 1110 West Green Street, Urbana, Illinois 61801
(Received 23 June 1988)

The InSb(100) surface was grown using the techniques of molecular-beam expitaxy. The surface was found to undergo several surface reconstructions, including a $c(4\times4)$, a $c(8\times2)$, an asymmetric (1×3), a symmetric (1×3), and a (1×1). High-resolution photoemission spectra of the In and Sb 4*d* core levels clearly exhibited surface-shifted components for some of these reconstructed surfaces. Analyses of the In and Sb core-level photoemission intensities as well as of the surface to bulk intensity ratios for the $c(4\times4)$ and $c(8\times2)$ structures were carried out. The $c(4\times4)$ surface was found to be terminated with $1-\frac{3}{4}$ monolayers of Sb, while $\frac{3}{4}$ monolayer of In was found to be the termination of the $c(8\times2)$ surface. Structural models are proposed for the $c(8\times2)$ and $c(4\times4)$ based upon these coverages and upon existing models of the similar GaAs(100) structures.

I. INTRODUCTION

Molecular-beam-epitaxy (MBE) techniques have to some extent made possible the fabrication of custom-tailored structures such as semiconductor heterojunctions and superlattices. MBE can also be used to modify surface structures. For the III-V compound semiconductors, different surface reconstructions can be produced by varying the substrate temperature and the ratio between the arrival rates for the anion and cation material.[1-9] In this study, we use high-energy electron diffraction (HEED) and synchrotron photoemission spectroscopy to probe the surface structure and composition of the (100) surface of the III-V compound semiconductor InSb.

Previous HEED studies of the InSb(100) surface have shown several surface reconstructions, including a (1×1), a $c(8\times2)$ an asymmetric (1×3), a (4×3), a (5×7), and a $(2\sqrt{2}\times2\sqrt{2})R45°$.[8,9] There is some disagreement in the literature about whether the latter structure should be designated as $(2\sqrt{2}\times2\sqrt{2})R45°$ or rather $(\sqrt{2}\times\sqrt{2})R45°$ or simply (2×2).[8,9] We were able to reproduce the phase diagrams compiled by Oe, Ando, and Siguiyama,[8] and by Noreika, Francombe, and Wood,[9] with only slight discrepancies in temperature. Our HEED analysis indicates that the structure in question is definitely the $(2\sqrt{2}\times2\sqrt{2})R45°$ as discussed by Oe, Ando, and Sugiyama.[8] Another name for this structure is $c(4\times4)$, and we will use this less cumbersome notation in this article. We were not able to generate the (5×7) structure, but we did generate a symmetric (1×3) structure in the same region of the phase diagram that Noreika, Francombe, and Wood,[9] observed the (5×7). The (4×3) reconstruction does not appear to be a separate structure, but rather a mixture of domains of the asymmetric (1×3) and $c(8\times2)$ structures. For this reason, we do not report on this structure.

The various InSb(100) surface reconstructions have in many cases also been observed for several other III-V compounds. The material that has been studied by far the most is GaAs(100).[1-3,10] Our results for the InSb(100) reconstructions show stoichiometry similar to observations of the GaAs(100) reconstructions. Several models have been developed for the $c(8\times2)$, $c(2\times8)$, and $c(4\times4)$ structures that have been observed for the GaAs(100) surface.[3,10-12] We have adapted these models to describe the InSb(100) $c(4\times4)$ and $c(8\times2)$ surfaces.

II. EXPERIMENT

InSb(100) substrates were obtained from Metal Specialties Inc. (Fairfield, CT), oriented 3° off the [100] direction toward the [011] direction. Samples were mechanochemically polished in this orientation using a 0.05% bromine in methanol solution. Samples were attached to a molybdenum heating block, and placed in the photoemission vacuum chamber. Several cycles of ion sputtering with 500-eV Ar ions and annealing at 400 °C were sufficient to obtain clean, ordered $c(8\times2)$ surfaces which were used as the starting surfaces for MBE growth. MBE was conduced *in situ* using a quartz-crystal thickness monitor to measure evaporation rates. In was evaporated from a tungsten crucible heated by electron beam bombardment. Sb was evaporated from a boron-nitride effusion cell. Substrate temperatures were monitored using a Chromel-Alumel thermocouple attached to the sample back. HEED was used to determine the surface reconstructions that were generated.

Photoemission experiments were conducted at the Synchrotron Radiation Center (Stoughton, WI) of the University of Wisconsin–Madison using the 1-GeV storage ring Aladdin. The University of Illinois extended-range grasshopper monochromator was used to select photon energies for the experiments. An angle-integrated geometry was employed for all spectra. In order to obtain a high degree of surface sensitivity, photon energies of 58 and 72 eV were used to observe the In 4*d* and Sb 4*d* core levels, respectively. Binding energies were referenced to the Fermi level as measured from a gold foil in electrical contact with the sample. Spectra of the Fermi edge indicated that our overall instrumental resolution

for the high-resolution spectra was approximately 0.25 eV.

III. RESULTS

A. MBE and HEED

The $c(4\times4)$ structure was generated by exposing the InSb to an Sb flux while holding the InSb substrate at temperatures between 260 °C and 360 °C, consistent with the phase diagrams of Oe, Ando, and Sugiyama,[8] and of Noreika, Francombe, and Wood.[9] Since the amount of Sb evaporated was sufficient to produce much more than a monolayer coverage (1 monolayer $=4.76\times10^{14}$ atoms/cm^2), the Sb coverage must reach a saturation point. This behavior has also been observed for As on the GaAs(100)-$c(4\times4)$.[3,4,6,10] In order to obtain the highest quality $c(4\times4)$ reconstruction, the surface structure was monitored with HEED during evaporation of Sb with the substrate temperature held at 260 °C. After the $c(4\times4)$ pattern was developed as determined by HEED, the Sb shutter was closed and the substrate heater was turned off. The $c(4\times4)$ surface is most definitely Sb-rich by nature of the preparation procedure.

The $c(8\times2)$ structure could be generated both by MBE and by sputtering and annealing, but the best-quality HEED patterns were produced only with MBE and annealing with temperatures between 350 °C and 400 °C. A high-quality $c(8\times2)$ reconstruction could also be produced by evaporating approximately 1 monolayer of In on a surface that was initially $c(4\times4)$ (Sb-rich), with the temperature held in the 350 °C–400 °C range. These results indicate that the $c(8\times2)$ surface is most likely In-rich.

The asymmetric (1×3) structure seems to have an intermediate surface stoichiometry between the Sb-rich $c(4\times4)$ surface and the In-rich $c(8\times2)$ surface. It could be generated by annealing the $c(4\times4)$ surface between 360 °C and 420 °C; presumably, the annealing process drives off some Sb from the surface. Alternately, it could be generated by evaporating Sb on the $c(8\times2)$ surface in this temperature range. The HEED pattern for this surface was not nearly as sharp as those for the $c(8\times2)$ and $c(4\times4)$ surfaces. The asymmetric label is given to this pattern because the $\frac{1}{3}$-order HEED streaks are significantly closer together than would be observed for a standard (1×3) pattern.[8,9]

The symmetric (1×3) and (1×1) structures were generated with Sb flux and substrate temperatures less than 250 °C. Photoemission intensity measurements indicate that the (1×3) surface is extremely Sb-rich (>2 monolayers of Sb on the surface), and that the (1×1) surface is more Sb-rich than the (1×3) surface. HEED shows both these structures to have very poor ordering. Since only the $c(8\times2)$ and $c(4\times4)$ structures produced very high-quality HEED patterns, further analyses deal primarily with those two surfaces.

B. Intensity measurements

Low-resolution photoemission spectra of the $c(4\times4)$ and $c(8\times2)$ surfaces were taken using a photon energy of 90 eV. In each spectrum, both the In and Sb core levels were recorded. An analysis of the In and Sb 4*d* core-level intensities based upon the usual layer-attenuation model was carried out to determine surface stoichiometry of the two surfaces. Several cases for the surface termination of the two surfaces were considered.

Case 1. The $c(8\times2)$ surface is terminated by a fraction of a monolayer of In, α, and the $c(4\times4)$ surface is terminated by a fraction of a monolayer of Sb, β, where both α and β are between 0 and 1. The In and Sb core-level intensities for the $c(4\times4)$ surface can be expressed as follows:

$$I(\mathrm{In})/I_1=\beta(e^{-d/l}+e^{-3d/l}+\cdots)+(1-\beta)(1+e^{-2d/l}+\cdots), \quad (1)$$

$$I(\mathrm{Sb})/I_2=\beta(1+e^{-2d/l}+\cdots)+(1-\beta)(e^{-d/l}+e^{-3d/l}+\cdots). \quad (2)$$

In Eqs. (1) and (2), I_1 and I_2 represent the intensity contribution from a single layer of In and Sb atoms, respectively. The other parameters in the equations are the escape depth l, of the electrons, and the spacing d between atomic planes in InSb(100). A similar set of equations can be written for the $c(8\times2)$ surface:

$$I'(\mathrm{In})/I_1=\alpha(1+e^{-2d/l}+\cdots)+(1-\alpha)(e^{-d/l}+e^{3d/l}+\cdots), \quad (3)$$

$$I'(\mathrm{Sb})/I_2=\alpha(e^{-d/l}+e^{-3d/l}+\cdots)+(1-\alpha)(1-e^{-2d/l}+\cdots). \quad (4)$$

The photoemission intensities are affected by the sample positioning accuracy in front of the photoelectron analyzer after sample preparation and the time-dependent decay of the storage-ring current. The latter problem can to some extent be corrected by normalizing the measured intensities to storage-ring beam current, but the photon intensity is not exactly proportional to the beam current. A more accurate measurement can be accomplished by simply using the ratio between the In and Sb intensities for a given spectrum, avoiding the above problems. By dividing Eq. (1) by Eq. (2) and Eq. (3) by Eq. (4), we obtain the In/Sb core-level intensity ratios, R and R', for the $c(4\times4)$ and $c(8\times2)$ surfaces, respectively,

$$R=(I_1/I_2)(\beta e^{-d/l}+1-\beta)[\beta+(1-\beta)e^{-d/l}]^{-1}, \quad (5)$$

$$R'=(I_1/I_2)[\alpha+(1-\alpha)e^{-d/l}](\alpha e^{-d/l}+1-\alpha)^{-1}. \quad (6)$$

Dividing Eq. (5) by Eq. (6) removes the dependence upon I_1/I_2. Solving for β in terms of α yields the following relationship:

$$\beta=\frac{\alpha(1-e^{-d/l})(R'/R+e^{-d/l})-(R'/R-e^{-2d/l})}{(1-e^{-d/l})[\alpha(1-e^{-d/l})(R'/R-1)-(R'/R+e^{-d/l})]}. \quad (7)$$

The value of R'/R is measured to be 1.97 ± 0.04; the uncertainty reflects measurements made from several sample surfaces. For reasonable values of the mean free path l, there is no combination of α and β that satisfy Eq. (7) such that $0<\alpha<1$ and $0<\beta<1$. Therefore, other cases need be considered in which more than one monolayer of In or Sb terminates the surface.

Case 2. The $c(8\times2)$ surface is still terminated by a fraction of a monolayer of In, α, as in case 1; the $c(4\times4)$ surface is terminated by $(1+\beta)$ monolayers of Sb, where again β is between 0 and 1. The In and Sb core-level intensities for the $c(8\times2)$ surface can still be expressed as in Eqs. (3) and (4). Equations (1) and (2) for the $c(4\times4)$ surface must be modified for this case as shown in Eqs. (8) and (9):

$$I(\mathrm{In})/I_1=\beta(e^{-2d/l}+e^{-4d/l}+\cdots)+(1-\beta)(e^{-d/l}+e^{-3d/l}+\cdots)\ , \tag{8}$$

$$I(\mathrm{Sb})/I_2=\beta(e^{-d/l}+e^{-3d/l}+\cdots)+(1-\beta)(e^{-2d/l}+e^{-4d/l}+\cdots)+1\ . \tag{9}$$

By doing manipulations similar to that shown for case 1, we obtain

$$\beta=\frac{\alpha(1-e^{-d/l})(R'/R+e^{d/l})-(R'/R-1)}{(1-e^{-d/l})[\alpha(1-e^{-d/l})(R'/R-1)-(R'/R+e^{-d/l})]}\ . \tag{10}$$

Case 3. The $c(4\times4)$ surface is terminated by a fraction of a monolayer of Sb, β, as in case 1, and the $c(8\times2)$ surface is terminated by $1+\alpha$ monolayers of In where α lies between 0 and 1. The relationship between β and α becomes

$$\beta=\frac{\alpha(1-e^{-d/l})(R'/R+e^{-d/l})-(R'/R-1)}{(1-e^{-d/l})[\alpha(1-e^{-d/l})(R'/R-1)-(R'/R+e^{d/l})]}\ . \tag{11}$$

Case 4. The $c(4\times4)$ surface is terminated by $1+\beta$ monolayers of Sn and the $c(8\times2)$ surface is terminated by $1+\alpha$ monolayers of In; again both α and β are between 0 and 1. We obtain

$$\beta=\frac{\alpha(1-e^{-d/l})(R'/R+e^{d/l})-(R'/R-e^{2d/l})}{(1-e^{-d/l})[\alpha(1-e^{-d/l})(R'/R-1)-(R'/R+e^{d/l})]}\ . \tag{12}$$

Equations (10)–(12) were evaluated using the experimental values of R'/R ranging from 1.93 to 2.01 and assuming the mean free path to be between 6.0 and 6.5 Å for a photon energy of 90 eV. The value of d for InSb(100) is 1.623 Å ($\frac{1}{4}$ of the lattice constant). The results are summarized in Fig. 1. The range of possible coverages for the $c(4\times4)$ and $c(8\times2)$ surfaces is given by the region between the two curves in Fig. 1.

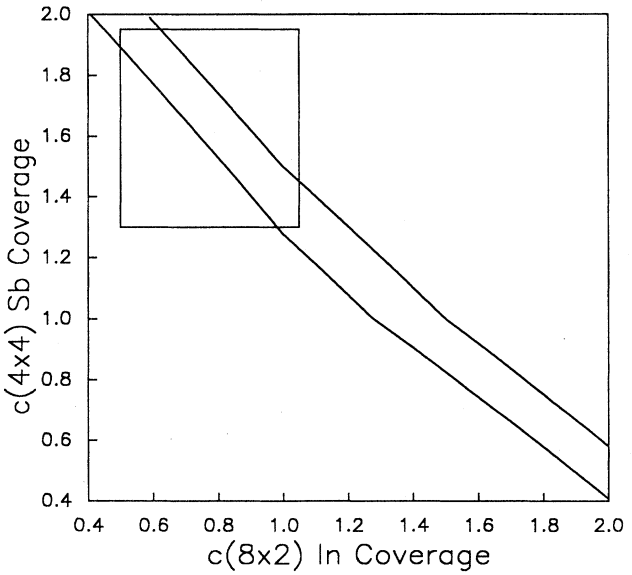

FIG. 1. Results of the photoemission intensity analysis for the $c(4\times4)$ and $c(8\times2)$ surfaces. The vertical axis represents the Sb coverage for the $c(4\times4)$ surface, and the horizontal axis represents the In coverage for the $c(8\times2)$ surface. The pair of coverages for the two surface lies between the two curves inside the rectangular region.

The range of possible surface stoichiometries can be further reduced by directly comparing intensities from two different spectra, one obtained from the $c(4\times4)$ surface and the other from the $c(8\times2)$ surface. The relevant quantities here are $r(\mathrm{In})\equiv I'(\mathrm{In})/I(\mathrm{In})$ and $r(\mathrm{Sb})\equiv I'(\mathrm{Sb})/I(\mathrm{Sb})$. As mentioned earlier, the procedure will have errors from the storage-ring beam current as well as from reproducing sample position after surface preparation. Several independent sets of measurements were taken so that the error can be estimated. Using the assumptions of case 2 (above), the following expressions for α and β can be derived:

$$\alpha=\frac{r(\mathrm{In})/r(\mathrm{Sb})-1+[1-r(\mathrm{In})](1+e^{-d/l})}{[r(\mathrm{In})/r(\mathrm{Sb})-1](1-e^{-d/l})}\ , \tag{13}$$

$$\beta=\frac{r(\mathrm{In})/r(\mathrm{Sb})-1+[1-1/r(\mathrm{Sb})](1+e^{d/l})}{[r(\mathrm{In})/r(\mathrm{Sb})-1](1-e^{-d/l})}\ . \tag{14}$$

Similar expressions can be written for the other cases, but measured intensities produce no pairs of α and β such that $0<\alpha<1$ and $0<\beta<1$. Putting the photoemission intensities from several measurements into Eqs. (13) and (14) indicates that the values of α and β lie within the rectangular region indicated in Fig. 1.

C. Core-level line-shape analysis

High-resolution angle-integrated photoemission spectra of the In $4d$ and Sb $4d$ core levels for the $c(4\times4)$, $c(8\times2)$, and the asymmetric (1×3) surfaces were fit with Voigt line shapes. Details of the nonlinear least-squares-fitting technique can be found elsewhere.[13–16]

For the following figures, the fitted curves are indicated by the solid lines passing through data points represented by dots. For the cases in which a surface-shifted component is present, the fitted curves are broken down into the surface and bulk components and displayed just below each core-level spectrum.

Figure 2 shows spectra of the Sb 4*d* core level of InSb(100)-*c*(4×4) recorded using two different photon energies. The 72-eV spectrum is much more surface sensitive than the 54-eV spectrum because of escape depth considerations.[13–19] By comparing these two spectra, it is clear that there is a surface component in addition to the bulk component. The surface and bulk components obtained from the fit are labeled *S* and *B*, respectively, in Fig. 2. The spin-orbit splitting, intensity branching ratio between $4d_{3/2}$ and $4d_{5/2}$ contributions, and the Lorentzian width (not the Gaussian width) were constrained to be the same for both components in the fit. Pertinent fitting parameters are listed in Table I.

Figure 3 shows the intensity ratio between the surface and bulk components for Sb 4*d* core-level spectra recorded with a variety of different photon energies; this ratio reflects the surface sensitivity of the measurement. The ratio peaks around 70–80 eV (corresponding to photoelectron kinetic energies of about 35–45 eV), implying that the photoelectron escape depth is the shortest at these energies.

The surface-sensitive In 4*d* core-level spectrum for the *c*(4×4) surface is shown in Fig. 4. There is no surface-shifted component that is apparent. A single spin-orbit component was sufficient to produce a very good fit to the data. Fitting parameters can be found in Table I.

Figure 5 shows a set of Sb 4*d* core-level spectra for the *c*(8×2) surface similar to that shown for the *c*(4×4) surface. Here, only one spin-orbit split component was needed to obtain a good fit to the data. Table I shows the pertinent fitting parameters. The peak width did not decrease as surface sensitivity was decreased as would be expected if there were actually a significant surface-shifted contribution to the spectra. This implies that surface shifts, if present, are very small.

Figure 6 displays the In 4*d* core-level spectrum for the *c*(8×2) structure. A single component was adequate to produce a fair fit to the data; the fitting parameters are displayed in Table I. However, the overall peak width is significantly larger than that for the *c*(4×4) case indicating the presence of a surface component. Attempts to incorporate an additional component failed to produce a unique, reproducible fit. Thus, although a surface component must be present, the binding energy shift is too small to resolve.

Figure 7 shows the Sb 4*d* core-level spectra for the asymmetric (1×3) surface. Although fairly good fits for the Sb 4*d* could be obtained with a single component, the

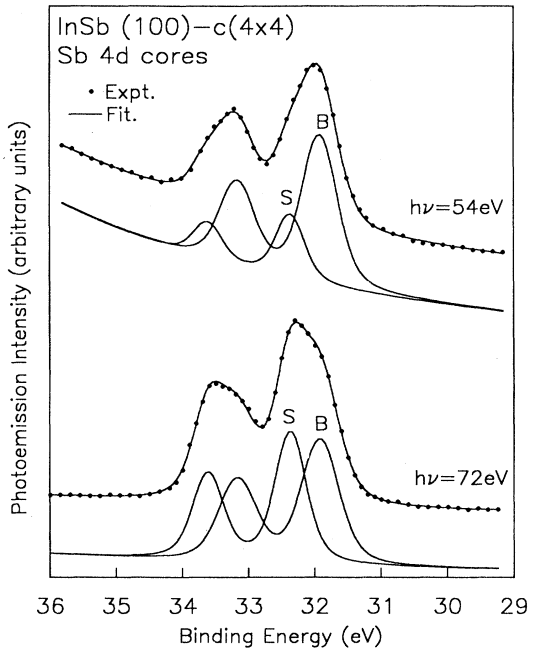

FIG. 2. Angle-integrated photoemission spectra of the Sb 4*d* core level for the *c*(4×4) surface reconstruction recorded with photon energies of 54 and 72 eV. The dots represent data points, and the curves through the dots are fits to the data. The surface (*S*) and bulk (*B*) components comprising each fit are shown just below each spectrum. The binding-energy scale is referenced to the Fermi level.

TABLE I. Line-shape parameters resulting from fits of the Sb 4*d* core-level data for the various surfaces studied. All energies are in units of eV. Binding energies are referenced to the Fermi level. The branching ratio is the intensity ratio between the $4d_{5/2}$ and $4d_{3/2}$ spin-orbit-split components. All parameters are for fits of the In 4*d* and Sb 4*d* spectra recorded using photon energies of 58 eV and 72 eV, respectively.

	c (4×4)		*c* (8×2)		Asymmetric (1×3)	
	In	Sb	In	Sb	In	Sb
$4d_{5/2}$ binding energy	17.45	31.92	17.33	31.63	17.36	31.87
Spin-orbit splitting	0.86	1.25	0.88	1.25	0.88	1.25
Branching ratio	1.62	1.53	1.48	1.39	1.56	1.46
Surface shift		−0.45			−0.37	
Surface-to-bulk intensity ratio		0.89			0.18	
Gaussian width						
bulk	0.39	0.54	0.58	0.56	0.43	0.73
surface		0.42			0.43	
Lorentzian width	0.25	0.25	0.14	0.19	0.19	0.25

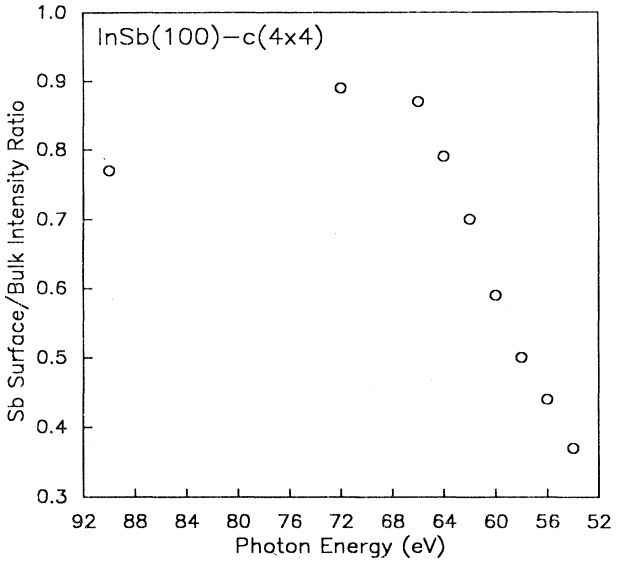

FIG. 3. Surface-to-bulk photoemission intensity ratio for the Sb 4*d* core level for the $c(4\times4)$ surface as a function of photon energy. The data points are indicated by the open circles.

Gaussian width decreased significantly as surface sensitivity was decreased. This indicates that there is one or more unresolved surface components incorporated in the line shape. Again, an attempt to incorporate more than a single component failed to produce unique, reasonable fitting parameters.

Figure 8 shows the In 4*d* core-level spectra for the asymmetric (1×3) surface. A small surface-shifted com-

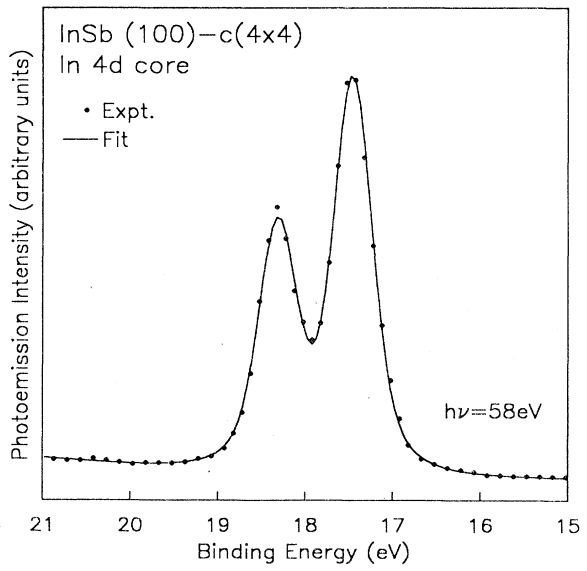

FIG. 4. Angle-integrated photoemission spectrum of the In 4*d* core level for the $c(4\times4)$ surface reconstruction. The dots represent data points, and the curve through the dots is a fit to the data. No surface component was observed for the spectrum. The binding-energy scale is referenced to the Fermi level.

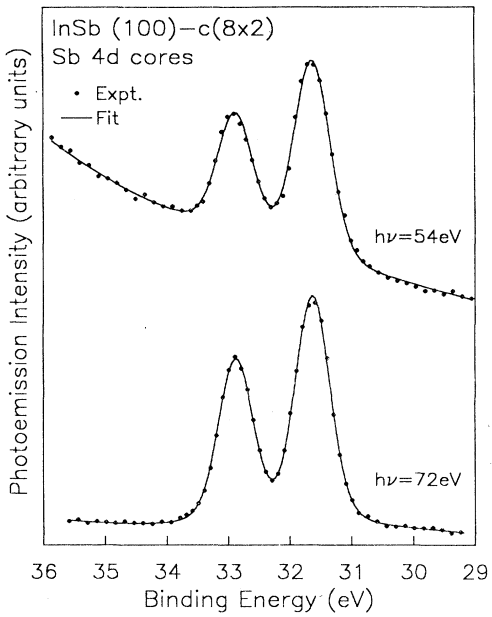

FIG. 5. Angle-integrated photoemission spectra of the Sb 4*d* core level for the $c(8\times2)$ surface reconstruction recorded with photon energies of 54 and 72 eV. The dots represent data points, and the curves through the dots are fits to the data. No surface component was observed for these spectra. The binding-energy scale is referenced to the Fermi level.

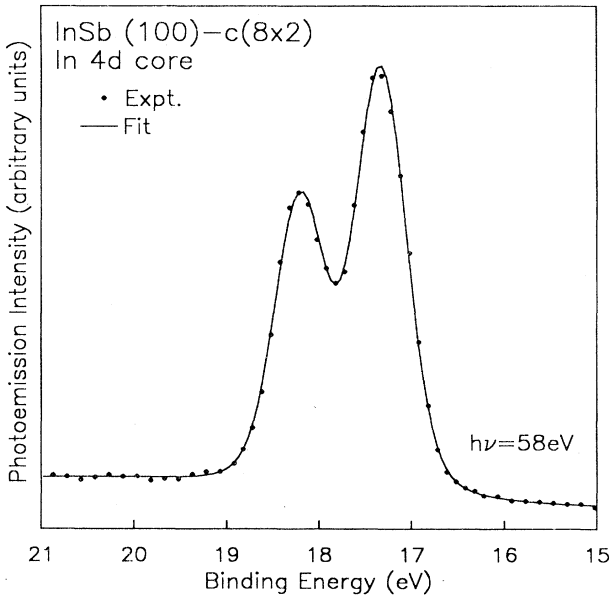

FIG. 6. Angle-integrated photoemission spectrum of the In 4*d* core level for the $c(8\times2)$ surface reconstruction. The dots represent data points, and the curve through the dots is a single-component fit to the data. The surface shift is too small to resolve. The binding-energy scale is referenced to the Fermi level.

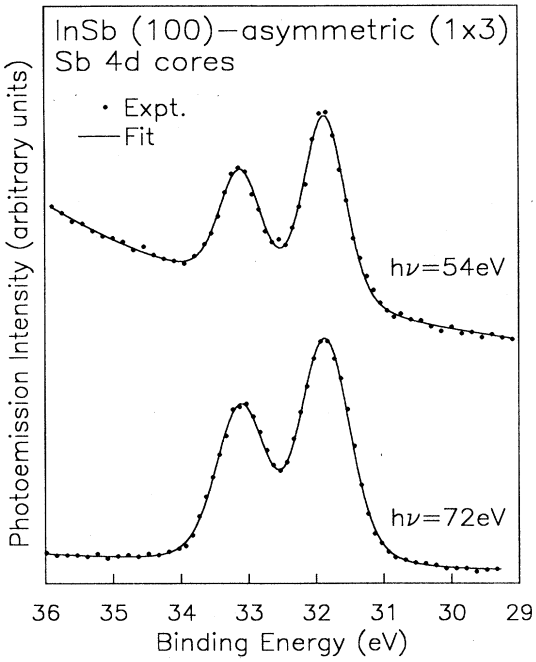

FIG. 7. Angle-integrated photoemission spectra of the Sb 4*d* core level for the asymmetric (1×3) surface reconstruction recorded with photon energies of 54 and 72 eV. The dots represent data points, and the curves through the dots are fits to the data. No surface component was used to fit these spectra, although the change in width with photon energy indicates the presence of surface shifts (too small to resolve). The binding-energy scale is referenced to the Fermi level.

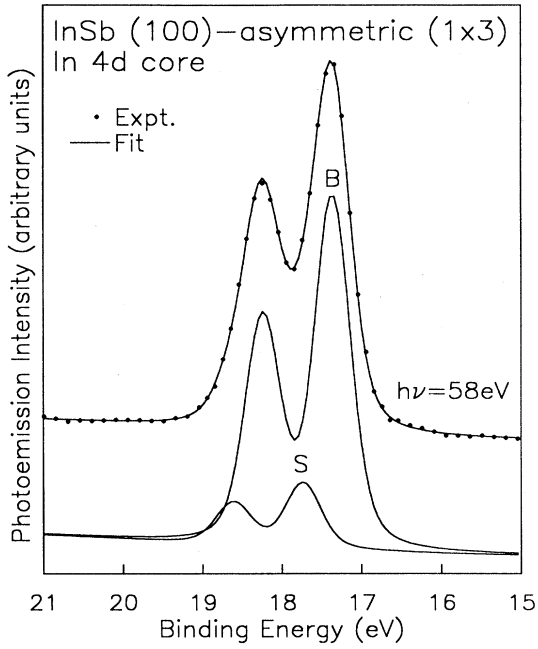

FIG. 8. Angle-integrated photoemission spectra of the In 4*d* core level for the asymmetric (1×3) surface reconstruction. The dots represent data points, and the curve through the dots is a fit to the data. The surface (*S*) and bulk (*B*) components are shown. The binding-energy scale is referenced to the Fermi level.

ponent was necessary to account for the tail on the high binding-energy side of the line shape. Fitting parameters are listed in Table I. Since both the In 4*d* and Sn 4*d* core levels show some sort of surface feature, the asymmetric (1×3) surface is most likely terminated by a mixture of In and Sb. The poor quality and asymmetry of the HEED pattern for this structure indicates that this structure is not well ordered. For these reasons no model is proposed for the asymmetric (1×3) structure.

D. Surface-structure models

The intensity analysis discussed above indicates that the $c(4\times4)$ surface is terminated by between 1.30 and 1.95 monolayers of Sb (Fig. 1). Several structural models were considered for the $c(4\times4)$ surface based upon this range of Sb coverages. Figure 9 shows the only one of these models that is commensurate with the results of the Sb 4*d* core-level line-shape analysis (see below). This model calls for $1-\frac{3}{4}$ monolayers of Sb on the surface; $\frac{3}{4}$ monolayers of Sb form dimers on top of a monolayer-Sb-terminated surface. This coverage is consistent with some reports for the As coverage on the GaAs(100)-$c(4\times4)$ surface.[3]

Note that in the above intensity analysis, only the total intensity (bulk plus surface) was used. Additional information can be obtained by considering the surface-to-bulk intensity ratio for a given core level. It is reasonable to assume that the surface contribution to the $c(4\times4)$ Sb 4*d* core-level line shape is derived from all of the exposed atoms on the surface (atoms that are three-fold coordinated). This includes the $\frac{3}{4}$-monolayer Sb dimers on the surface and the $\frac{1}{2}$-monolayer Sb atoms in the next layer down near the dimer vacancies. The dimer atoms will contribute a photoemission intensity of $\frac{3}{4}I_2$. The contribution from the $\frac{1}{2}$-monolayer Sb atoms in the next layer near the dimer vacancies will be partially attenuated by the dimer atoms. Since the blockage by the dimers

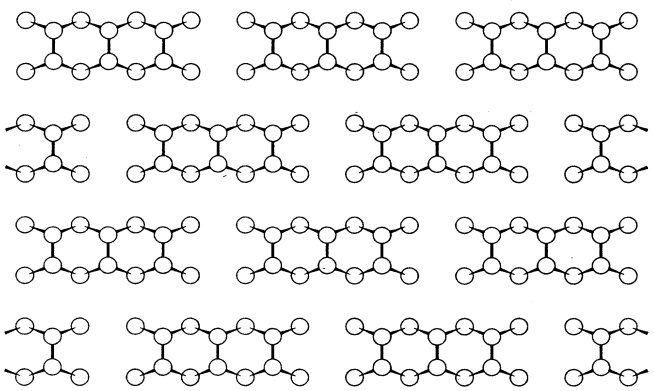

FIG. 9. Illustration of the proposed model of the $c(4\times4)$ superstructure. All circles represent Sb atoms; only the top $1-\frac{3}{4}$ monolayers are shown.

occurs only on one side for each of these atoms, the emission intensity for them is taken to be the average of the intensity for an unattenuated $\frac{1}{2}$ monolayer and the intensity for $\frac{1}{2}$ monolayer attenuated by one full monolayer. The expression for the total intensity of the surface component becomes

$$I_s = \tfrac{3}{4}I_2 + \tfrac{1}{2}[(I_2/2) + (I_2/2)e^{-d/l}] . \quad (15)$$

Likewise, for the bulk intensity contribution,

$$I_B = \tfrac{1}{2}I_2 e^{-d/l} + \tfrac{3}{4}I_2(e^{-3d/l} + e^{-5d/l} + \cdots) + \tfrac{1}{4}I_2(e^{-2d/l} + e^{-4d/l} + \cdots) . \quad (16)$$

Dividing Eq. (15) by Eq. (16) gives the expression for the surface-to-bulk intensity ratio:

$$\frac{I_s}{I_B} = \frac{(e^{d/l} + \frac{1}{4})(e^{2d/l} - 1)}{\frac{1}{4}(1 + e^{d/l}) + \frac{1}{2}e^{2d/l}} . \quad (17)$$

Evaluating Eq. (17) for values of electron escape depth between 5.0 and 5.5 Å gives values of the surface to bulk intensity ratio ranging from 0.81 to 0.96. The measured value (from Table I) of 0.89 is well within this range, so this model is consistent with both intensity and line-shape analyses. In this model, there are no surface In atoms; therefore, no surface shift for the In core is expected and none is observed (Fig. 4).

Assuming a value of $1-\frac{3}{4}$ monolayers for the Sb coverage on the $c(4\times4)$ surface, the In coverage for the $c(8\times2)$ surface must fall between the 0.62 and 0.79 monolayer, as indicated by Fig. 1. A value of $\frac{3}{4}$ monolayer is well within this range and is in agreement with a previously proposed model for Ga on the GaAs(100)-$c(8\times2)$ and for As on the GaAs(100)-$c(2\times8)$.[10,20] Figure 10 is an illustration of this model for In on the InSb(100)-$c(8\times2)$. The structure consists of $\frac{3}{4}$ monolayer of In dimers on a monolayer-Sb-terminated surface. This $\frac{3}{4}$ monolayer of surface In dimers could exhibit a surface shift. The experimental results indicate that a small, unresolved shift is present, but the relative intensity of the surface component cannot be reliably deduced from the data. The surface Sb atoms near the In dimer vacancies could also show a surface shift, but no significant surface shifts are observed experimentally. Note that the Sb surface shift in this case is not necessarily the same as that for the Sb atoms near the dimer vacancies in the $c(4\times4)$ case discussed above because the Sb atoms are bonded to different kinds of dimer atoms in these two cases. It is conceivable that the shift in the $c(8\times2)$ case happens to be small (e.g., due to differences in electrostatic energies),[21] but a detailed theoretical analysis of the electronic properties is required to answer this question.

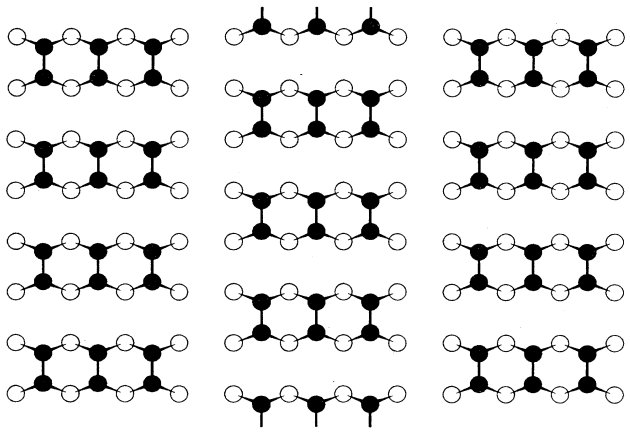

FIG. 10. Illustration of the proposed model of the $c(8\times2)$ superstructure. Only the top $1-\frac{3}{4}$ monolayers are shown. Open circles represent the full monolayer of Sb atoms; while the closed circles represent the $\frac{3}{4}$ monolayer of dimer-bonded In atoms.

E. Accuracy of the analyses

In our analysis of the core-level photoemission intensities, the usual layer-attenuation model based on the phenomenological electron escape depth was used. This simple model has some inherent error or uncertainty. In the use of the surface-to-bulk intensity ratios of individual core-level spectra, the analysis is also uncertain due to the surface reconstruction. For example, a small change in spacing between the first and second atomic layers could affect the photoemission-intensity ratio. These are well-known problems in using core-level spectroscopy for surface-stoichiometry determination. Without detailed knowledge of the atomic structures of these surfaces, we are not able to construct a better, more accurate model. However, we believe that the errors are not large, and these errors are effectively taken into account in our work by allowing the electron escape depth to be somewhat uncertain. The good correlation between our analyses based on different measurements and the proposed structural models strongly supports our conclusions.

IV. SUMMARY

MBE techniques were used to generate various reconstructions on the InSb(100) surface following established procedures. Photoemission intensity measurements of the surface stoichiometry indicated that the $c(8\times2)$ surface was most In-rich, followed by the asymmetric (1×3), the $c(4\times4)$, the (1×3), and the (1×1) surfaces in that order. Line-shape analyses of the Sb 4*d* and In 4*d* core levels, coupled with the intensity analyses indicated that the $c(4\times4)$ surface is terminated with $1-\frac{3}{4}$ monolayers of Sb atoms and that the $c(8\times2)$ surface is terminated with $\frac{3}{4}$ monolayer of In atoms. Based on these coverages, models are proposed for both structures which have $\frac{3}{4}$ monolayer of dimer bonded atoms on the surface along with $\frac{1}{4}$ monolayer of dimer vacancies. These models are similar to those proposed for the similarly reconstructed GaAs(100) surfaces.

ACKNOWLEDGMENTS

This material is based upon work supported by the U.S. Department of Energy (Division of Materials Sciences, Office of Basic Energy Sciences) under Contract

No. DE-AC02-76ER01198. Some of the personnel and equipment support was also derived from grants from the National Science Foundation (Grant Nos. DMR-83-52083 and DMR-86-14234), the IBM Thomas J. Watson Research Center (Yorktown Heights, NY), and the E. I. du Pont de Nemours and Company (Wilmington, DE). The Synchrotron Radiation Center of the University of Wisconsin–Madison is supported by the National Science Foundation under Contract No. DMR-80-20164. We acknowledge the use of central facilities of the Materials Research Laboratory of the University of Illinois, which is supported by the U.S. Department of Energy (Division of Materials Sciences, Office of Basic Energy Sciences) under Contract No. DE-AC02-76ER01198, and the National Science Foundation under Contract No. DMR-86-12860.

[1]A. Y. Cho, J. Appl. Phys. **47**, 2841 (1976).
[2]P. Drathen, W. Ranke, and K. Jacobi, Surf. Sci. **77**, L162 (1978).
[3]P. K. Larsen, J. H. Neave, J. F. van der Veen, P. J. Dobson, and B. A. Joyce, Phys. Rev. B **27**, 4966 (1983).
[4]R. Z. Bachrach, R. S. Bauer, P. Chiardia, and G. V. Hansson, J. Vac. Sci. Technol. **19**, 335 (1981).
[5]R. Ludeke, IBM J. Res. Dev. **22**, 304 (1978).
[6]T.-C. Chiang, R. Ludeke, M. Aono, G. Landgren, F. J. Himpsel, and D. E. Eastman, Phys. Rev. B **27**, 4770 (1983).
[7]R. Ludeke, T.-C. Chiang, and D. E. Eastman, Physica B+C **117&118B**, 819 (1983).
[8]K. Oe, S. Ando, and K. Sugiyama, Jpn. J. Appl. Phys. **19**, L417 (1980).
[9]A. J. Noreika, M. H. Francombe, and C. E. C. Wood, J. Appl. Phys. **52**, 7416 (1981).
[10]J. P. Harbison and H. H. Farrell, J. Vac. Sci. Technol. B **6**, 733 (1988).
[11]P. J. Dobson, J. H. Neave, and B. A. Joyce, Surf. Sci. **119**, L339 (1982).
[12]D. J. Chadi, C. Tanner, and J. Ihm, Surf. Sci. **120**, L425 (1982).
[13]C. R. Brundle, J. Vac. Sci. Technol. **11**, 212 (1974).
[14]T. Miller, F. Rosenwinkel, and T.-C. Chiang, Solid State Commun. **47**, 935 (1983); Phys. Rev. B **30**, 570 (1984).
[15]T. Miller, T. C. Hsieh, and T.-C. Chiang, Phys. Rev. B **33**, 6983 (1986).
[16]T.-C. Chiang, Comments At. Mol. Phys. **13**, 299 (1983).
[17]T. Miller, A. P. Shapiro, and T.-C. Chiang, Phys. Rev. B **31**, 7915 (1985).
[18]P. John, T. Miller, T. C. Hsieh, A. P. Shapiro, A. L. Wachs, and T.-C. Chiang, Phys. Rev. B **34**, 6704 (1986).
[19]P. John, F. M. Leibsle, T. Miller, T. C. Hsieh, and T.-C. Chiang, Superlatt. Microstruct. **3**, 347 (1987).
[20]M. D. Pashley, K. W. Haberen, W. Friday, J. M. Woodall, and P. D. Kirchner, Phys. Rev. Lett. **60**, 2176 (1988).
[21]R. E. Watson, J. W. Davenport, M. L. Perlman, and T. K. Sham, Phys. Rev. B **24**, 1791 (1981).